This is an open access article published under a Creative Commons Attribution (CC-BY) License, which permits unrestricted use, distribution and reproduction in any medium, provided the author and source are cited.

ACS AUTHORCHOICE

analytical chemistry

pubs.acs.org/ac Article

Narrowband Modulation Two-Dimensional Mass Spectrometry and Label-Free Relative Quantification of Histone Peptides

Matthias Halper, Marc-André Delsuc, Kathrin Breuker, and Maria A. van Agthoven*

Cite This: *Anal. Chem.* 2020, 92, 13945−13952 Read Online

ACCESS | Metrics & More | Article Recommendations | Supporting Information

ABSTRACT: Two-dimensional mass spectrometry (2D MS) on a Fourier transform ion cyclotron resonance (FT-ICR) mass analyzer allows for tandem mass spectrometry without requiring ion isolation. In the ICR cell, the precursor ion radii are modulated before fragmentation, which results in modulation of the abundance of their fragments. The resulting 2D mass spectrum enables a correlation between the precursor and fragment ions. In a standard broadband 2D MS, the range of precursor ion cyclotron frequencies is determined by the lowest mass-to-charge (m/z) ratio to be fragmented in the 2D MS experiment, which leads to precursor ion m/z ranges that are much wider than necessary, thereby limiting the resolving power for precursor ions and the accuracy of the correlation between the precursor and fragment ions. We present narrowband modulation 2D MS, which increases the precursor ion resolving power by reducing the precursor ion m/z range, with the aim of resolving the fragment ion patterns of overlapping isotopic distributions. In this proof-of-concept study, we compare broadband and narrowband modulation 2D mass spectra of an equimolar mixture of histone peptide isoforms. In narrowband modulation 2D MS, we were able to separate the fragment ion patterns of all ^{13}C isotopes of the different histone peptide forms. We further demonstrate the potential of narrowband 2D MS for label-free quantification of peptides.

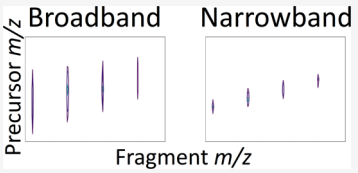

INTRODUCTION

Histones are 11−21 kDa proteins that make up the chief components of chromatin, the complex around which DNA is wound in the nucleus.[1] Histones frequently carry numerous post-translational modifications (PTMs), which have been found to play a central role in gene regulation, DNA repair, chromosome condensation, and spermatogenesis. A functional understanding of histone modifications and the proposed "histone code" requires far more experimental data than are available so far.[2]

Mass spectrometry (MS) is ideally suited to address this challenge as it can directly detect all mass-altering modifications and does not require laborious biochemical techniques for analysis. Specifically, MS can provide mass values of both the biomolecules under study and their fragments from dissociation in tandem mass spectrometry (MS/MS) experiments, for which prefractionation by chromatography is typically required.[3,4] However, it is often challenging—if not impossible—to fractionate very similar compounds, for example, post-translationally modified proteins that differ only in their modification patterns. Likewise, standard MS/MS experiments, in which each ionized compound (precursor ion) in a sample is isolated before dissociation and detection of its fragment ions in the mass spectrometer, can be limited by overlapping isotopic distributions of different peptide or protein forms. Although isolation and fragmentation of a single histone isoform,[5] as well as the label-free, direct localization and relative quantitation of histone[6−8] and ribonucleic acid,[8] modifications by MS/MS have been demonstrated, a more general approach that does not rely on precursor ion isolation would significantly advance all fields of PTM research.

Two-dimensional mass spectrometry (2D MS) is a method for Tandem MS that enables the correlation between the precursor and fragment ions without ion isolation.[9−11] 2D MS is a useful technique for samples that are difficult to separate through chromatographic methods, such as protein isoforms with relatively small modifications (e.g., methylations). Another advantage of 2D MS is the fact that all analytes are subjected to the same experimental conditions, which makes 2D MS a good candidate to perform quantification studies.

2D MS can be performed on Fourier transform ion cyclotron resonance (FT-ICR) or linear ion trap mass spectrometers and has been successfully applied to the analysis of small molecules, polymers, and in bottom-up and top-down proteomics.[12−23] In most studies using 2D MS, the analytes were within an m/z range of several hundred units. In the case of modified histones, the m/z range is typically less than 10 units depending on the charge state of the protein.

High-resolution mass spectrometers, that is, the FT-ICR mass spectrometer and Orbitrap, are used to resolve complex fragmentation patterns of, for example, large peptides or

Received: July 3, 2020
Accepted: September 22, 2020
Published: September 22, 2020

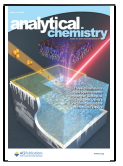

ACS Publications © 2020 American Chemical Society

proteins, with high mass accuracy.[24−26] Efficient 2D MS in a FT-ICR mass spectrometer requires a gas-free fragmentation method such as infrared multiphoton dissociation, which preferentially fragments the most labile bonds including those of the PTMs of peptides and proteins, or electron capture dissociation (ECD), which preferentially fragments the C-α backbone bonds of peptides and proteins.[27−29] These characteristics make ECD the method of choice for PTM analysis of peptides and proteins in 2D MS.[30]

In standard broadband 2D MS, the cyclotron frequency range for precursor ions is determined by the lowest m/z ions to be fragmented in the 2D MS experiment, which leads to m/z ranges that are much wider than necessary, thereby limiting the resolving power of the precursor ions (corresponding to the isolation m/z window in standard MS/MS). In one-dimensional FT-ICR MS, heterodyne or "narrowband" techniques have been developed to enable ultrahigh resolution.[31−33] We present narrowband modulation 2D MS, which is conceptually different from one-dimensional narrowband MS and does not use heterodyne detection. Narrowband modulation 2D MS increases the precursor ion resolving power with the aim of differentiating the fragmentation patterns of overlapping isotopic distributions (e.g., peptides and proteins with and without disulfide bonds).

In this study, we compare the analysis of histone peptide isoforms with broadband and narrowband modulation 2D MS. We further discuss the use of 2D MS for the localization and assignment of PTMs, as well as their relative quantification. In order to simplify this article, narrowband modulation 2D MS will be referred to as "narrowband 2D MS", although this is not meant to indicate an equivalence to one-dimensional narrowband MS techniques.

EXPERIMENTAL METHODS

Sample Preparation. Milli-Q water (Merck Millipore, Darmstadt), methanol, and acetic acid (VWR, Vienna, Austria) were used in all experiments. As model peptides, C-terminal GK-biotinylated histone H3 sequences (amino acid residues 21 to 44) without and with native modifications (mono-, di-, and trimethylation) at K27 were purchased (AnaSpec, Fremont, CA, USA) with a purity of >95%, in which K27 of the full-length histone corresponds to K7 of the model peptides.

Peptides were desalted using MWCO 2000 Vivaspin centrifugal concentrators (Sartorius, Göttingen, Germany) at 7900 rcf, 6× ammonium acetate 100 mM (Sigma, Vienna, Austria), and 6× H_2O. Peptide concentration was determined by UV absorption at 280 nm using an Implen Nano PhotometerTM (Implen, München, Germany). For electrospray ionization, equimolar mixtures (0.1 μM each) of unmodified (referred to as "wild-type" in the text), mono-, di-, and trimethylated peptides (referred to as "K7 1m", "K7 2m", and "K7 3m", respectively) in 50:50 H_2O/CH_3OH and 1% vol CH_3COOH, pH ∼ 3.0 were prepared from 100 μM stock solutions of each peptide in H_2O.

Instrument Parameters. 2D mass spectra were acquired on a 7 T Apex Ultra FT-ICR mass spectrometer (Bruker Daltonik, GmbH, Bremen, Germany) with an electrospray ion source operated in the positive mode and direct injection at a flow rate of 90 μL/h. Ions were accumulated for 0.1 s in the first hexapole and 0.1 s in the second hexapole.[34] In the quadrupole, ions were isolated at m/z 490 with an isolation window of m/z 30 and transferred to the Infinity ICR cell through a series of focusing lenses.[35]

The experimental script for the acquisition of 2D mass spectra is shown in Scheme 1. All excitation pulses (P_1, P_2, and P_3) have a frequency range of 357,144.31−71,669.99 Hz (corresponding to m/z 301.08−1500).

Scheme 1. . Experimental Script of 2D MS

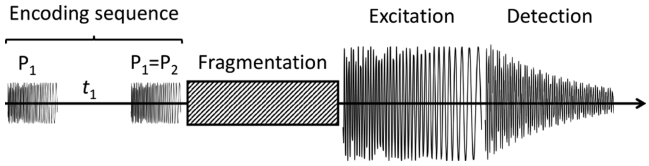

The frequency list was composed of 458 frequencies with a 624.71 Hz decrement. For the encoding pulses P_1 and P_2, the power level (corresponding to the amplitude of the pulses) was set at 106 V_{pp} with a pulse length of 1.0 μs per frequency. For the excitation pulse P_3, the power level was set at 80 V_{pp} with a pulse length of 20 μs per frequency (default settings in the Apex Control software, Bruker Daltonik, GmbH, Bremen, Germany).[36] The fragmentation mode used was ECD, using a hollow cathode.[37] The heater was at 1.3 A, the lens at 20 V, the ECD bias at 2.0 V, and the irradiation pulse at 0.03 s. The transients were recorded with 1 Mwords (16 bits) for 1.4680 s, with a 714,288.62 Hz sampling frequency.

For the broadband 2D mass spectrum, the encoding period t_1 was incremented 4096 times with a 2.0 μs increment, leading to a 250 kHz Nyquist frequency (mass range: m/z 334.439−1500 with the high m/z limit set by the frequency range of P_1). The longest encoding period was 8.192 ms. For the narrowband 2D mass spectrum, the encoding period t_1 was incremented 4096 times with an 8.0 μs increment, leading to a 62.5 kHz Nyquist frequency (mass range: m/z 415.00−546.825). The longest encoding period was 32.768 ms. For neither 2D mass spectrum was the detection heterodyne.

Data Processing. The 2D mass spectra were processed and visualized using the SPIKE software developed independently by the University of Strasbourg and CASC4DE (Illkirch-Graffenstaden, France) in a 64-bit Python 3.7 programming language on an open-source platform distributed by the Python Software Foundation (Beaverton, OR, USA).[38] Processed data files were saved using the HDF5 file format. Both 2D mass spectra were digitally demodulated with a demodulation frequency of 71,669.99 Hz and denoised using the support selection for noise elimination (SANE) algorithm with a SANE rank of 50.[10,39−41]

For the broadband 2D mass spectrum, cyclotron frequencies in the vertical precursor ion dimension were calculated using the following equation

$$f_{ICR} = f + f_0 \quad (1)$$

in which f_{ICR} is the reduced cyclotron frequency of the precursor ion, f is the measured modulation frequency of the precursor ion, and f_0 is the lowest frequency in the excitation pulses (71,669.99 Hz). For the narrowband 2D mass spectrum, cyclotron frequencies in the vertical precursor ion dimension were calculated using the following equation

$$f_{ICR} = f + f_0 + 2f_N \quad (2)$$

https://dx.doi.org/10.1021/acs.analchem.0c02843
Anal. Chem. 2020, 92, 13945−13952

Scheme 2. Schematics of 2D Mass Spectra Obtained in Broadband (Left) and Narrowband Mode (Right)

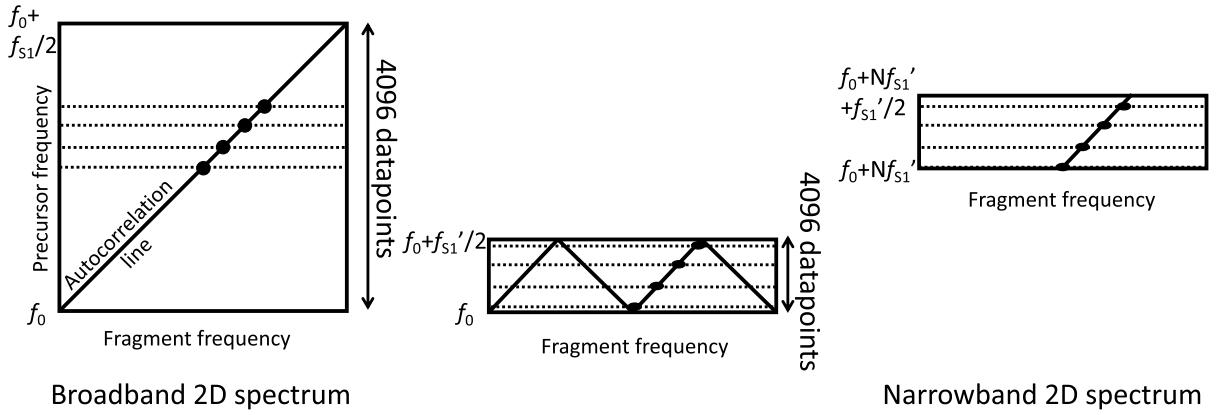

in which f_N is the Nyquist frequency in the vertical precursor ion dimension (62,500.00 Hz).

Each 2D mass spectrum was internally calibrated in the horizontal fragment ion m/z dimension using a quadratic frequency-to-mass conversion.[42] For each precursor ion species, four to five fragment ion spectra with the highest fragment ion intensities were added before peak-picking.

Theory of Narrowband 2D MS. Scheme 1 shows the experimental script for 2D FT-ICR MS. A detailed description of the mechanisms of the experiment can be found in previous articles.[10,43,44] The radius modulation of precursor ions at the end of the encoding sequence can be modeled according to the incremental delay t_1

$$r(t_1) = r_0\sqrt{2(1 + \cos 2\pi(f_{ICR} - f_0)(t_1 - T))} \quad (3)$$

in which r is the radius of the ion packet in the ICR cell after the encoding sequence, r_0 is the radius of the ion packet at the end of the first pulse, f_{ICR} is the reduced cyclotron frequency of the precursor ion, f_0 is the lowest frequency in the encoding pulses, and T is the duration of the first encoding pulse.[9,10,43,44]

Scheme 2 (left) shows the schematic of a broadband 2D spectrum in the frequency domain. The modulation frequency in the vertical precursor frequency is $f_{ICR}-f_0$. The highest modulation frequency f_{max1} in the vertical dimension is determined by the encoding period (t_1 in Scheme 1) increment Δt_1

$$f_{max1} = \frac{1}{2}f_{S1} = \frac{1}{2\Delta t_1} \quad (4)$$

in which f_{S1} is the sampling frequency in the vertical precursor dimension. As a result, the range of precursor cyclotron frequencies in the 2D spectrum is $[f_0, f_{S1}/2]$.

According to the Shannon–Nyquist theorem, periodically sampling a signal at a sampling frequency of f_S produces an aliasing of the signal frequencies such that all frequencies f_N separated by f_S of a multiple of f_S produce the same measurement f[45]

$$f_N = \pm(f + Nf_S), \qquad N \in \mathbb{Z} \quad (5)$$

The ± sign is due to the cosine in the modulation equation for 2D MS.[10,43] Signals in 2D MS experiments that have frequencies higher than $f_{S1}/2$ can therefore be represented in aliased form in the 2D spectrum.

In Scheme 2 (left), the autocorrelation line has modulation signals up to $f_{S1}/2$ (precursor ion cyclotron frequencies are between f_0 and $f_0 + f_{S1}/2$). If the sampling frequency is reduced in the experiment by increasing the encoding period increment Δt_1 (Scheme 2 center), then the autocorrelation line is aliased and can be folded back into the spectrum multiple times and appears to zig–zag.

The sampling frequency f_{S1}' and the lowest excitation frequency f_0 can be chosen so that the modulation frequency range of interest is folded back into the spectrum an even number of times. The precursor ion cyclotron frequencies can be recovered by offsetting all frequencies in the precursor ion dimension by $N f_{S1}'$, where N is the number of times that the signal of interest has been folded back into the spectrum (Scheme 2 right). Subsequent frequency-to-mass conversion yields the narrowband 2D mass spectrum. Although folding over the signal does not truncate the precursor mass range, in practice quadrupole isolation is desirable for effective data analysis.

In cases where only a small m/z range is necessary in the vertical precursor ion dimension, such as a single charge state of a protein and its isoforms, narrowband 2D MS significantly reduces the vertical precursor m/z range, which significantly increases the resolving power of each peak in the vertical precursor ion dimension and enables more accurate precursor–fragment correlation.

The total acquisition time of a 2D MS experiment is proportional to the number of t_1 increments. As a result, narrowband 2D MS can either be used to increase the vertical resolving power by keeping a constant number of data points, or decreasing experiment times and sample consumption and retaining the same resolving power.

RESULTS AND DISCUSSION

Figure 1 shows the full broadband (Figure 1a) and narrowband (Figure 1b) 2D mass spectra of a mixture of the four isoforms of the H3 histone peptide. In both 2D mass spectra, fragment ion m/z ratios are plotted horizontally. Precursor ion m/z ratios, calculated after conversion from measured frequencies to reduced cyclotron frequencies with eq 1 (broadband) and eq 2 (narrowband), are plotted vertically. In both 2D mass spectra, the autocorrelation line has been extracted and shows the isotopic distribution of the $[M + 6H]^{6+}$ ions of the four isoforms, evenly spaced by m/z 2.335942 (corresponding to 14.015652 Da for CH_2 divided by z = 6). Because of the quadrupole isolation, these species are the only ones detected on the autocorrelation line.

https://dx.doi.org/10.1021/acs.analchem.0c02843
Anal. Chem. 2020, 92, 13945–13952

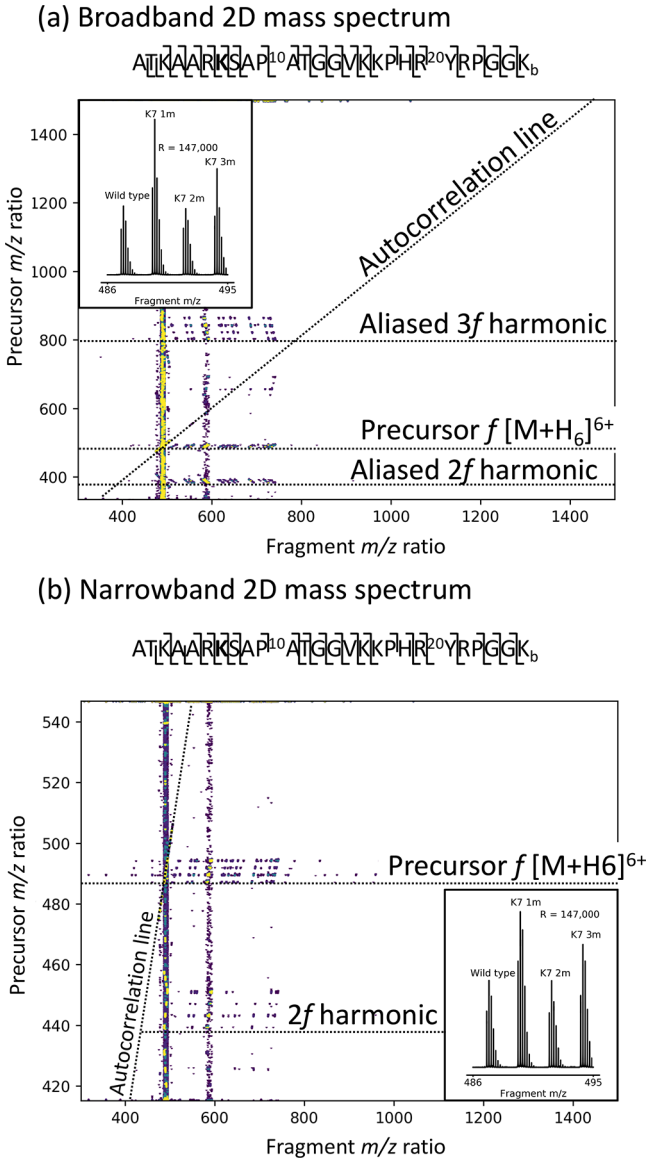

Figure 1. . (a) Broadband 2D ECD mass spectrum of histone peptide isoforms (wild-type, ^{7}K monomethylated or K7 1m, ^{7}K dimethylated or K7 2m, and ^{7}K trimethylated or K7 3m). Inset: extracted autocorrelation line, sequence coverage of wild-type histone peptide. (b) Narrowband 2D ECD mass spectrum of histone peptide isoforms (wild-type, ^{7}K monomethylated, ^{7}K dimethylated, and ^{7}K trimethylated). Inset: extracted autocorrelation line, sequence coverage of wild-type histone peptide.

The resolving power on the autocorrelation line is approximately 147,000 at m/z 490 in both 2D mass spectra.

In both 2D mass spectra, the ECD fragmentation patterns of the peptide isoforms are represented in the horizontal fragment ion spectra. The sequence coverage of the unmodified (wild-type) peptide is shown in Figure 1a,b for the respective 2D mass spectra. In both cases, the sequence coverage is nearly complete. The peak assignments for all fragment ion spectra can be found in the Supporting Information for the broadband 2D mass spectrum (Tables S1−S4) and the narrowband 2D mass spectrum (Tables S5−S8). The sequence coverage for all four isoforms can be found in Figure S1 of the Supporting Information for the broadband 2D mass spectrum and Figure S2 for the narrowband 2D mass spectrum. For all isoforms, in both 2D mass spectra, the sequence coverage is nearly complete (over 20 out of 25 cleavages).

In the broadband 2D mass spectrum, the vertical range is m/z 334.439−1500. Only 0.77% of the vertical m/z range contains analytically useful information (m/z 486−495 for precursor ions) because it is determined by the Nyquist frequency, which has to be higher than the cyclotron frequency of the lowest m/z ratio of interest. In the narrowband 2D mass spectrum, the vertical mass range is m/z 415.00−546.825, which means that 6.8% contains useful analytical information. In the narrowband 2D mass spectrum, the vertical m/z range is still determined by the Nyquist frequency, but the foldover effect is used to reduce it.

In both 2D mass spectra, vertical harmonics are clearly visible. The vertical harmonics, as well as residual scintillation noise, are clearly visible in the 2D mass spectra in Figure 1 because of the low relative abundance of fragment ion peaks compared to the precursor ion peaks in ECD.[40,46] The vertical harmonics in 2D mass spectra arise from the non-sinusoidal modulation of signals during the 2D MS experiment.[36,43,44,47] Their relative intensity can be minimized by adjusting the modulation zone in the ICR cell to the fragmentation zone during the encoding sequence (Scheme 1), but they cannot be eliminated.[36] A previous study has shown that a careful examination of the harmonics in precursor ion spectra can uncover additional peaks for those fragment ions whose fragmentation zones differ significantly from a Gaussian profile (e.g., in cases of secondary fragmentation or combined fragmentation methods, such as IR-ECD).[48]

In the narrowband 2D mass spectrum (Figure 1b), the 2f harmonic is visible (the 3f harmonic has a too low signal-to-noise ratio to be visible). The absence of precursor ion peaks on the autocorrelation line clearly marks the fragment ion spectra as harmonics. In the broadband 2D mass spectrum (Figure 1a), the aliased 2f and 3f harmonics are visible. The foldover effect is marked by the fact that, in both cases, the slopes of the dissociation lines are negative. The signal from vertical harmonics can be used, in a similar way to the signal from harmonics in one-dimensional FT-ICR mass spectra, to increase the resolving power in the vertical dimension and therefore to improve the accuracy of the precursor−fragment correlation.[49−51] Although the smaller mass range in the precursor ion dimension of narrowband 2D mass spectra may lead to a decrease in harmonic signals, they may be folded back into the spectrum by aliasing.

Figure 2 shows the vertical precursor ion spectra extracted from both the broadband and the narrowband 2D mass spectrum. Figure 2a shows the vertical precursor ion spectrum of the monoisotopic c_5 fragment at m/z 460.2879. Fragment c_5 does not contain any modification, and therefore, the precursor ion spectrum shows peaks for all four isoforms. In the vertical precursor ion spectrum extracted from the broadband 2D mass spectrum, the isotopic peaks of the four precursor ions of c_5 are not resolved (black circles show the theoretical isotopic peaks in the vertical dimension). In contrast, the isotopic distribution of the precursor ions is resolved in the precursor ion spectrum extracted from the narrowband 2D mass spectrum, albeit not to the baseline.

The vertical resolving power in both spectra can be calculated from the extracted precursor ion spectra shown in Figure 2b, which correspond to the monoisotopic z_{24}^{4+} fragment of the wild-type peptide at m/z 682.8849 (to help compare between the two peaks, the spectra have been

https://dx.doi.org/10.1021/acs.analchem.0c02843
Anal. Chem. 2020, 92, 13945−13952

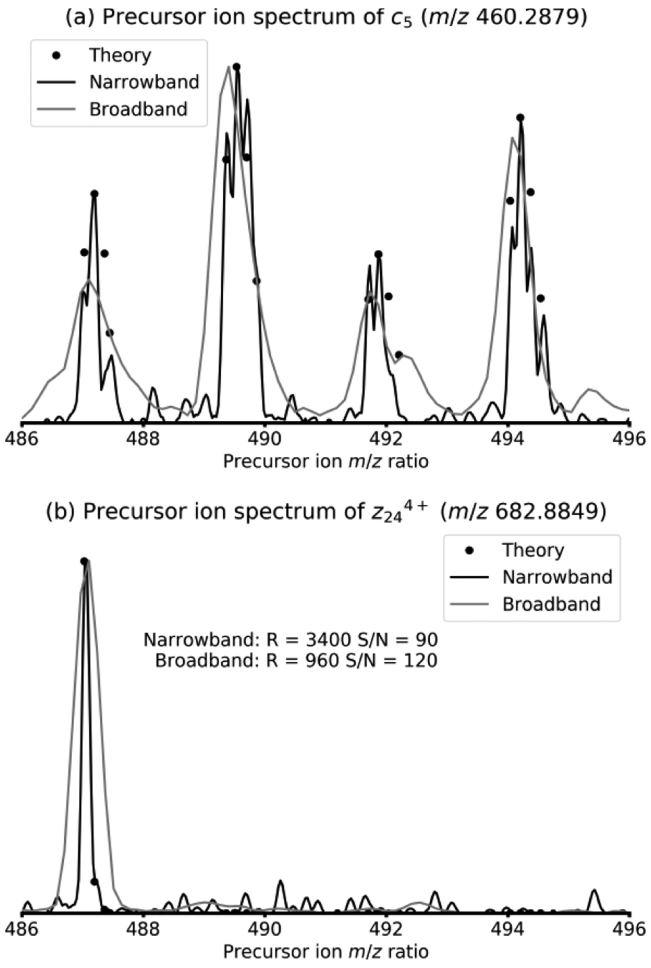

Figure 2. (a) Normalized precursor ion spectrum of c_5 extracted from the broadband and the narrowband 2D mass spectra (black dots: theoretical isotopic distribution). (b) Normalized precursor ion spectrum of z_{24}^{4+} extracted from the broadband and the narrowband 2D mass spectra at the first harmonic (black dots: theoretical isotopic distribution).

normalized, which makes the noise level of the spectrum extracted from the narrowband 2D mass spectrum appear higher).

The z_{24}^{4+} fragment contains the K7 residue on which all modifications (methylation, dimethylation, and trimethylation) are located, so the precursor ion spectrum only shows a peak for the wild-type peptide. In addition, the z_{24}^{4+} fragment contains 24 out of 26 residues. Any ^{13}C isotope in the precursor ion has a probability close to 100% to remain in the z_{24}^{4+} fragment instead of its complement c_2.[10,52] Therefore, the monoisotopic z_{24}^{4+} fragment is the product of the monoisotopic peak of the wild-type precursor with negligible contribution from any ^{13}C isotopes of the precursor ion, and the extracted precursor ion spectra in Figure 2b can be used to accurately determine the vertical resolving power and the accuracy of the precursor−fragment correlation.

The isotopic distributions of fragment ions in 2D mass spectra are further illustrated in Figure S4 in the Supporting Information.

As expected, the vertical resolving power in the narrowband 2D mass spectrum (3400 at m/z 487) is almost 4 times the vertical resolving power in the broadband 2D mass spectrum (960 at m/z 487). The vertical resolving power measures the accuracy of the precursor−fragment correlation. The horizontal resolving power corresponds to the standard resolving power of one-dimensional mass spectra. This result is consistent with the fact that the frequency range in the broadband 2D mass spectrum is 4 times the frequency range in the narrowband 2D mass spectrum with an equal number of data points in the vertical dimension.

Figure 3 shows the vertical precursor ion spectra of all four isotopes of the z_{24}^{4+} fragment of the $[M + 6H]^{6+}$ charge state of the wild-type histone peptide. Figure 3a shows the first harmonic peak (i.e., corresponding to the modulation frequency of the precursor ion radius) and Figure 3b shows its 2f harmonic peak (or second harmonic) with an adapted frequency-to-mass conversion as extracted from the broadband 2D mass spectrum. Figure 3c shows the first harmonic peak and Figure 3d shows its second harmonic peak as extracted from the narrowband 2D mass spectrum.

In Figure 3a (first harmonic of the broadband 2D mass spectrum), the isotopic distribution is not resolved (R = 960 for the ^{12}C isotopic peak). In Figure 3b, the use of the second harmonic enables an increase in revolving power (R = 2200), but the isotopic distribution is still not resolved. The signal-to-noise ratio is slightly lower for the second harmonic than in the first harmonic. The third harmonic is shown in the Supporting Information, Figure S5.

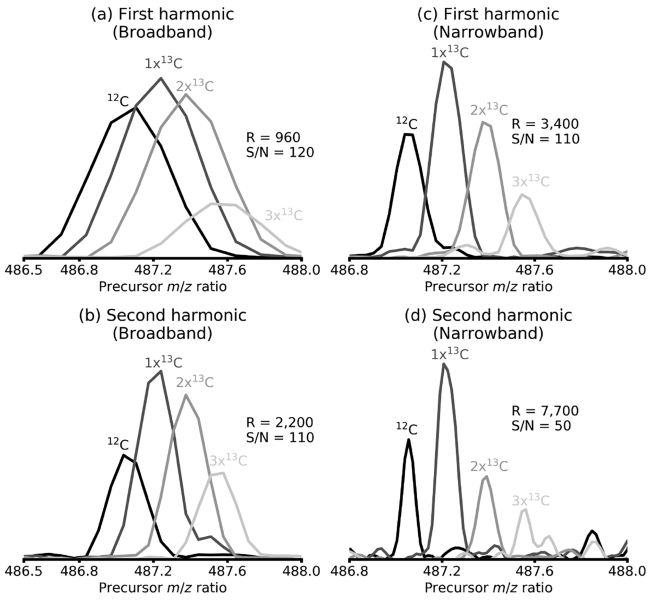

Figure 3. Precursor ion spectra of the isotopes of the z_{24}^{4+} fragment of the wild-type histone peptide, with frequency-to-mass conversion extracted from the broadband 2D mass spectrum for the (a) first harmonic peak and the (b) second harmonic peak and extracted from the narrowband 2D mass spectrum for the (c) first harmonic peak and the (d) second harmonic peak. The resolving power is measured on the ^{12}C isotopic peak, and the signal-to-noise ratio is measured for the 1 × ^{13}C isotopic peak.

In Figure 3c, while the isotopic distribution of the $[M + 6H]^{6+}$ precursor is resolved (R = 3400 for the ^{12}C isotopic peak), the peaks are not baseline-resolved. In Figure 3d, the isotopic distribution is resolved (R = 7700 for the ^{12}C isotopic peak). In the first harmonic, the signal-to-noise ratio of the 1 × ^{13}C isotopic peak was calculated to be 110, but in the second harmonic, it was calculated to be 50. The horizontal fragment

https://dx.doi.org/10.1021/acs.analchem.0c02843
Anal. Chem. 2020, 92, 13945−13952

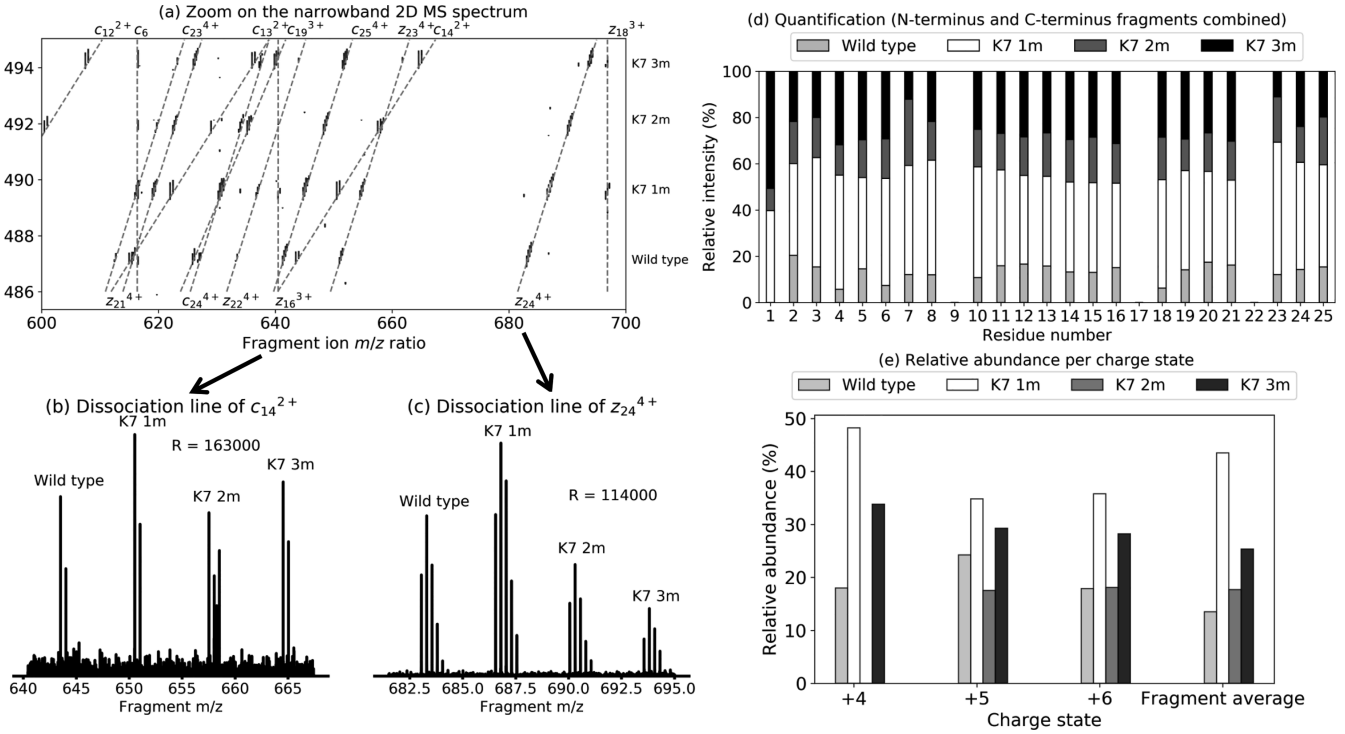

Figure 4. (a) Zoom-in of the narrowband 2D mass spectrum of the histone peptide mixture with various dissociation lines highlighted. (b) Extracted dissociation line of the c_{14}^{2+} fragment. (c) Extracted dissociation line of the z_{24}^{4+} fragment. (d) Label-free relative quantification of the four histone peptide isoforms using fragment abundances for each residue (N-terminus and C-terminus combined). (e) Label-free relative quantification of the four histone peptide isoforms using the relative abundances of each charge state (6+ precursor ion, 5+ and 4+ charge-reduced states) and average of the quantification using fragment ion abundances.

ion spectra for the second harmonic of all four isoforms (visible between vertical m/z 435−450 in Figure 1b) were peak-picked. The peak assignments are shown in the Supporting Information (Tables S9−S12).

The sequence coverage of all four isoforms in the second harmonic (Supporting Information Figure S3) was approximately 50%, compared to approximately 90% in the first harmonic. Unlike in one-dimensional FT-ICR MS, where the relative intensity of 2*f*−6*f* harmonics can be maximized by adapting the design of ICR cells,[49−51] increasing the relative intensity of higher harmonics in 2D FT-ICR MS comes at the expense of overall signal-to-noise ratio and thus analytical information.[36] However, in 2D MS, higher harmonics in the vertical dimension can be useful to establish precursor−fragment correlations when first harmonic fragment ion peaks have insufficient resolving power.

Figure 3 also highlights the necessity to add up fragment ion spectra in the narrowband 2D mass spectrum to obtain complete isotopic distributions. Further illustration can be found in Figure S6 in the Supporting Information.

Figure 4 shows how the narrowband 2D mass spectrum enables the sequencing of the four peptide isoforms, the identification and location of the modifications, and their relative quantification. Figure 4a shows a zoom-in of the narrowband 2D mass spectrum between m/z 600−700. For each peptide isoform, horizontal fragment ion spectra were extracted for each isotope and added up before peak-picking and peak assignment (Tables S5−S8 and Figure S2 in the Supporting Information).

Figure 4a illustrates how to locate peptide modifications. In the 2D mass spectrum, precursor ions of different m/z with fragments of identical m/z (i.e., fragments not containing the modified lysine) can all be found on the same vertical precursor ion spectrum. In Figure 4a, c_6 (m/z 616.3888), z_{16}^{3+} (m/z 640.3481), and z_{18}^{3+} (m/z 696.3790) all form vertical precursor ion spectra. Because the methylations are situated on residue number 7 counting from the N-terminus or residue number 19 counting from the C-terminus, these vertical precursor ion spectra enable the accurate localization of the modifications.

The complementary ions for fragments with identical m/z ratios can be found on diagonal dissociation lines following eq 6[10,16,48,53]

$$(m/z)_p = \frac{p}{n}(m/z)_f + \frac{\Delta m}{n} \quad (6)$$

in which $(m/z)_p$ is the m/z ratio of the precursor ion, $(m/z)_f$ is the m/z ratio of the fragment, n is the charge state of the precursor, p is the charge state of the fragment, and Δm is the mass difference between the precursor and the fragment. In Figure 4a, c_{12}^{2+}, c_{13}^{2+}, and c_{14}^{2+} are observed on dissociation lines with a slope of 2/6 = 0.33, c_{19}^{3+} on a dissociation line with a slope of 3/6 = 0.5 and finally z_{21}^{4+}, z_{22}^{4+}, z_{23}^{4+}, z_{24}^{4+}, c_{23}^{4+}, c_{24}^{4+}, and c_{25}^{4+} on dissociation lines with a slope of 4/6 = 0.67 (linear regressions available in Table S13 in the Supporting Information). The use of vertical precursor ion spectra and diagonal dissociation lines can therefore be used to locate the sites of peptide modifications.

Figure 4b,c shows the extracted dissociation lines of c_{14}^{2+} (Figure 4b) and z_{24}^{4+} (Figure 4c). The resolving power on both dissociation lines is sufficient to calculate the exact mass differences between the isoforms for correct assignments of the peptide modifications. In Figure 4b, the modifications are measured to have masses of 14.0155, 28.0313, and 42.0465 Da,

https://dx.doi.org/10.1021/acs.analchem.0c02843
Anal. Chem. 2020, 92, 13945−13952

corresponding to mono-, di-, and trimethylation, respectively. The unusual pattern for the K7 2m isotopic distribution results from the overlap of the c_{14}^{2+} and z_{23}^{4+} fragment ion distributions (see Figure 4a). Figure 4a–c therefore shows that a visual analysis of narrowband 2D mass spectra can be used for peptide sequencing and to identify and locate the modifications.

Figure 4d,e shows different methods to quantify the four peptide isoforms. In label-free relative quantification studies with one-dimensional MS/MS, relative intensities of ions with given mass differences are compared to locate modifications and quantify isoforms on one graph.[8,54] With 2D MS, locating modifications can be accomplished visually (cf. Figure 4a) and relative intensities can be plotted without distinguishing m/z ratios. In Figure 4d, the relative intensities are given for both N-terminus and C-terminus fragments.

Figure 4e shows the comparison of the quantification obtained by using peaks on the autocorrelation line (6+), the one-electron capture line (5+), the two-electron capture line (4+), and the average quantification used with the fragment ion peaks (fragment average). The proportions of the four peptide isoforms are consistent between all the four methods. The only discrepancy was in the proportions of the two-electron capture line, where K7 2m was not detected, because of the low abundance of the $[M + 6H]^{4+\bullet\bullet}$ charge state.

CONCLUSIONS

This study shows that decreasing the sampling frequency along the t_1 axis (i.e., precursor ion modulation) in 2D MS can substantially increase the resolving power in the vertical precursor ion m/z dimension for an unchanged acquisition time. Narrowband 2D MS can resolve isotopic distributions of the $[M + 6H]^{6+}$ ions in a mixture of four histone peptide isoforms (26 residues). The precursor–fragment correlation was high enough to enable the detailed examination of fragment isotopic distributions in the 2D mass spectrum. Finally, the study shows the capability of 2D MS to identify and locate histone modifications and to quantify their relative abundances.

As this study demonstrates, narrowband 2D MS has the potential for top-down MS of biomolecules. The high precursor–fragment correlation can be used to distinguish the fragmentation patterns of overlapping isotopic distributions (e.g., for proteins with and without disulfide bonds) and easily identify and locate modifications by extracting dissociation lines. The capacity of 2D MS to analyze all analytes in a sample with identical experimental parameters in a single experiment enables label-free relative quantification. These characteristics of 2D MS enable the analysis of heavily modified biomolecules, such as histones, for the elucidation of the histone code.[55]

ASSOCIATED CONTENT

Supporting Information

The Supporting Information is available free of charge at https://pubs.acs.org/doi/10.1021/acs.analchem.0c02843.

Peak assignment tables (broadband and narrowband 2D mass spectra), sequence coverage schemes (broadband and narrowband 2D mass spectra), slope and offset of dissociation lines, and isotopic distributions (PDF)

AUTHOR INFORMATION

Corresponding Author

Maria A. van Agthoven – *Institute for Organic Chemistry, University of Innsbruck, 6020 Innsbruck, Austria;* orcid.org/0000-0003-2438-3934; Email: maria.van-agthoven@uibk.ac.at

Authors

Matthias Halper – *Institute for Organic Chemistry, University of Innsbruck, 6020 Innsbruck, Austria*

Marc-André Delsuc – *Institut de Génétique et de Biologie Moléculaire et Cellulaire, INSERM U596, UMR 7104, Université de Strasbourg, 67404 Illkirch-Graffenstaden, France; CASC4DE, Pôle API, 67400 Illkirch-Graffenstaden, France;* orcid.org/0000-0002-1400-5326

Kathrin Breuker – *Institute for Organic Chemistry, University of Innsbruck, 6020 Innsbruck, Austria;* orcid.org/0000-0002-4978-0883

Complete contact information is available at: https://pubs.acs.org/10.1021/acs.analchem.0c02843

Author Contributions

The manuscript was written through contributions of all authors.

Notes

The authors declare no competing financial interest.

ACKNOWLEDGMENTS

M.A.v.A. dedicates this article to the memory of Christina M. Olsthoorn-de Munck. The authors thank Ms. Sarah Heel, Dr. Giovanni Calderisi, and Mr. Michael Palasser for helpful conversations. M.A.v.A. and K.B. thank Der Wissenschaftsfonds (Austrian Science Fund, FWF) for the Lise Meitner Fellowship project M 2757-B.

REFERENCES

(1) Peterson, C. L.; Laniel, M.-A. *Curr. Biol.* **2004**, *14*, R546–R551.
(2) Moradian, A.; Kalli, A.; Sweredoski, M. J.; Hess, S. *Proteomics* **2014**, *14*, 489–497.
(3) Taucher, M.; Breuker, K. *Angew. Chem., Int. Ed.* **2012**, *51*, 11289–11292.
(4) Tran, J. C.; Zamdborg, L.; Ahlf, D. R.; Lee, J. E.; Catherman, A. D.; Durbin, K. R.; Tipton, J. D.; Vellaichamy, A.; Kellie, J. F.; Li, M.; Wu, C.; Sweet, S. M. M.; Early, B. P.; Siuti, N.; LeDuc, R. D.; Compton, P. D.; Thomas, P. M.; Kelleher, N. L. *Nature* **2011**, *480*, 254–258.
(5) Smith, D. F.; Blakney, G. T.; Beu, S. C.; Anderson, L. C.; Weisbrod, C. R.; Hendrickson, C. L. *Anal. Chem.* **2020**, *92*, 3213–3219.
(6) Zheng, Y.; Fornelli, L.; Compton, P. D.; Sharma, S.; Canterbury, J.; Mullen, C.; Zabrouskov, V.; Fellers, R. T.; Thomas, P. M.; Licht, J. D.; Senko, M. W.; Kelleher, N. L. *Mol. Cell. Proteomics* **2016**, *15*, 776–790.
(7) Zheng, Y.; Huang, X.; Kelleher, N. L. *Curr. Opin. Chem. Biol.* **2016**, *33*, 142–150.
(8) Dang, X.; Singh, A.; Spetman, B. D.; Nolan, K. D.; Isaacs, J. S.; Dennis, J. H.; Dalton, S.; Marshall, A. G.; Young, N. L. *J. Proteome Res.* **2016**, *15*, 3196–3203.
(9) van Agthoven, M. A.; Delsuc, M.-A.; Bodenhausen, G.; Rolando, C. *Anal. Bioanal. Chem.* **2013**, *405*, 51–61.
(10) van Agthoven, M. A.; Lam, Y. P. Y.; O'Connor, P. B.; Rolando, C.; Delsuc, M.-A. *Eur. Biophys. J.* **2019**, *48*, 213–229.
(11) van Agthoven, M. A.; Delsuc, M.-A.; Rolando, C. *Int. J. Mass Spectrom.* **2011**, *306*, 196–203.

(12) van Agthoven, M. A.; O'Connor, P. B. *Rapid Commun. Mass Spectrom.* **2017**, *31*, 674−684.
(13) van Agthoven, M. A.; Barrow, M. P.; Chiron, L.; Coutouly, M.-A.; Kilgour, D.; Wootton, C. A.; Wei, J.; Soulby, A.; Delsuc, M.-A.; Rolando, C.; O'Connor, P. B. *J. Am. Soc. Mass Spectrom.* **2015**, *26*, 2105−2114.
(14) Simon, H. J.; van Agthoven, M. A.; Lam, P. Y.; Floris, F.; Chiron, L.; Delsuc, M.-A.; Rolando, C.; Barrow, M. P.; O'Connor, P. B. *Analyst* **2016**, *141*, 157−165.
(15) Floris, F.; van Agthoven, M.; Chiron, L.; Soulby, A. J.; Wootton, C. A.; Lam, Y. P. Y.; Barrow, M. P.; Delsuc, M.-A.; O'Connor, P. B. *J. Am. Soc. Mass Spectrom.* **2016**, *27*, 1531−1538.
(16) van Agthoven, M. A.; Wootton, C. A.; Chiron, L.; Coutouly, M.-A.; Soulby, A.; Wei, J.; Barrow, M. P.; Delsuc, M.-A.; Rolando, C.; O'Connor, P. B. *Anal. Chem.* **2016**, *88*, 4409−4417.
(17) Floris, F.; Vallotto, C.; Chiron, L.; Lynch, A. M.; Barrow, M. P.; Delsuc, M.-A.; O'Connor, P. B. *Anal. Chem.* **2017**, *89*, 9892−9899.
(18) Floris, F.; van Agthoven, M. A.; Chiron, L.; Wootton, C. A.; Lam, P. Y. Y.; Barrow, M. P.; Delsuc, M.-A.; O'Connor, P. B. *J. Am. Soc. Mass Spectrom.* **2018**, *29*, 207−210.
(19) Snyder, D. T.; Szalwinski, L. J.; Wells, J. M.; Cooks, R. G. *Analyst* **2018**, *143*, 5438−5452.
(20) Paris, J.; Morgan, T. E.; Wootton, C. A.; Barrow, M. P.; O'Hara, J.; O'Connor, P. B. *Anal. Chem.* **2020**, *92*, 6817−6821.
(21) Snyder, D. T.; Szalwinski, L. J.; St. John, Z.; Cooks, R. G. *Anal. Chem.* **2019**, *91*, 13752−13762.
(22) Szalwinski, L. J.; Holden, D. T.; Morato, N. M.; Cooks, R. G. *Anal. Chem.* **2020**, *92*, 10016−10023.
(23) Marzullo, B. P.; Morgan, T. E.; Wootton, C. A.; Perry, S. J.; Saeed, M.; Barrow, M. P.; O'Connor, P. B. *Anal. Chem.* **2020**, *92*, 11687−11695.
(24) Marshall, A. G.; Hendrickson, C. L.; Jackson, G. S. *Mass Spectrom. Rev.* **1998**, *17*, 1−35.
(25) Jonathan Amster, I. *J. Mass Spectrom.* **1996**, *31*, 1325−1337.
(26) Denisov, E.; Damoc, E.; Lange, O.; Makarov, A. *Int. J. Mass Spectrom.* **2012**, *325*−*327*, 80−85.
(27) Little, D. P.; Speir, J. P.; Senko, M. W.; O'Connor, P. B.; McLafferty, F. W. *Anal. Chem.* **1994**, *66*, 2809−2815.
(28) Zubarev, R. A.; Kelleher, N. L.; McLafferty, F. W. *J. Am. Chem. Soc.* **1998**, *120*, 3265−3266.
(29) Håkansson, K.; Cooper, H. J.; Emmett, M. R.; Costello, C. E.; Marshall, A. G.; Nilsson, C. L. *Anal. Chem.* **2001**, *73*, 4530−4536.
(30) Domon, B.; Aebersold, R. *Science* **2006**, *312*, 212−217.
(31) Drader, J. J.; Shi, S. D.-H.; Blakney, G. T.; Hendrickson, C. L.; Laude, D. A.; Marshall, A. G. *Anal. Chem.* **1999**, *71*, 4758−4763.
(32) Fujiwara, M.; Katakura, H.; Inoue, M. *Rapid Commun. Mass Spectrom.* **1990**, *4*, 237−238.
(33) Wei, J.; Antzutkin, O. N.; Filippov, A. V.; Iuga, D.; Lam, P. Y.; Barrow, M. P.; Dupree, R.; Brown, S. P.; O'Connor, P. B. *Biochemistry* **2016**, *55*, 2065−2068.
(34) Taucher, M.; Rieder, U.; Breuker, K. *J. Am. Soc. Mass Spectrom.* **2010**, *21*, 278−285.
(35) Caravatti, P.; Allemann, M. *Org. Mass Spectrom.* **1991**, *26*, 514−518.
(36) van Agthoven, M. A.; Chiron, L.; Coutouly, M.-A.; Sehgal, A. A.; Pelupessy, P.; Delsuc, M.-A.; Rolando, C. *Int. J. Mass Spectrom.* **2014**, *370*, 114−124.
(37) Tsybin, Y. O.; Witt, M.; Baykut, G.; Kjeldsen, F.; Håkansson, P. *Rapid Commun. Mass Spectrom.* **2003**, *17*, 1759−1768.
(38) Chiron, L.; Coutouly, M.-A.; Starck, J.-P.; Rolando, C.; Delsuc, M.-A. SPIKE a processing software dedicated to Fourier spectroscopies. **2016**, arXiv preprint arXiv:1608.06777, 1−13.
(39) Chiron, L.; van Agthoven, M. A.; Kieffer, B.; Rolando, C.; Delsuc, M.-A. *Proc. Natl. Acad. Sci. U.S.A.* **2014**, *111*, 1385−1390.
(40) van Agthoven, M. A.; Coutouly, M.-A.; Rolando, C.; Delsuc, M.-A. *Rapid Commun. Mass Spectrom.* **2011**, *25*, 1609−1616.
(41) Bray, F.; Bouclon, J.; Chiron, L.; Witt, M.; Delsuc, M.-A.; Rolando, C. *Anal. Chem.* **2017**, *89*, 8589−8593.
(42) Ledford, E. B., Jr.; Rempel, D. L.; Gross, M. L. *Anal. Chem.* **1984**, *56*, 2744−2748.
(43) Guan, S.; Jones, P. R. *J. Chem. Phys.* **1989**, *91*, 5291−5295.
(44) Pfandler, P.; Bodenhausen, G.; Rapin, J.; Walser, M. E.; Gäumann, T. *J. Am. Chem. Soc.* **1988**, *110*, 5625−5628.
(45) Jerri, A. J. *Proc. - IEEE* **1977**, *65*, 1565−1596.
(46) Zubarev, R. A.; Horn, D. M.; Fridriksson, E. K.; Kelleher, N. L.; Kruger, N. A.; Lewis, M. A.; Carpenter, B. K.; McLafferty, F. W. *Anal. Chem.* **2000**, *72*, 563−573.
(47) van Agthoven, M. A.; Kilgour, D. P. A.; Lynch, A. M.; Barrow, M. P.; Morgan, T. E.; Wootton, C. A.; Chiron, L.; Delsuc, M.-A.; O'Connor, P. B. *J. Am. Soc. Mass Spectrom.* **2019**, *30*, 2594−2607.
(48) van Agthoven, M. A.; Lynch, A. M.; Morgan, T. E.; Wootton, C. A.; Lam, Y. P. Y.; Chiron, L.; Barrow, M. P.; Delsuc, M.-A.; O'Connor, P. B. *Anal. Chem.* **2018**, *90*, 3496−3504.
(49) Grosshans, P. B.; Marshall, A. G. *Int. J. Mass Spectrom. Ion Processes* **1991**, *107*, 49−81.
(50) Vorobyev, A.; Gorshkov, M. V.; Tsybin, Y. O. *Int. J. Mass Spectrom.* **2011**, *306*, 227−231.
(51) Park, S.-G.; Anderson, G. A.; Bruce, J. E. *J. Am. Soc. Mass Spectrom.* **2020**, *31*, 719−726.
(52) O'Connor, P. B.; Little, D. P.; McLafferty, F. W. *Anal. Chem.* **1996**, *68*, 542−545.
(53) van Agthoven, M. A.; Chiron, L.; Coutouly, M.-A.; Delsuc, M.-A.; Rolando, C. *Anal. Chem.* **2012**, *84*, 5589−5595.
(54) Glasner, H.; Riml, C.; Micura, R.; Breuker, K. *Nucleic Acids Res.* **2017**, *45*, 8014−8025.
(55) Jenuwein, T.; Allis, C. D. *Science* **2001**, *293*, 1074−1080.

https://dx.doi.org/10.1021/acs.analchem.0c02843
Anal. Chem. 2020, 92, 13945−13952